photonics

MDPI

Communication

Point-by-Point Induced High Birefringence Polymer Optical Fiber Bragg Grating for Strain Measurement

Shixin Gao [1], Heng Wang [1,*], Yuhang Chen [2,3], Heming Wei [4], Getinet Woyessa [5], Ole Bang [5], Rui Min [6], Hang Qu [2,3], Christophe Caucheteur [7] and Xuehao Hu [7]

1 College of Science, Shenyang Aerospace University, Shenyang 110136, China
2 Research Center for Advanced Optics and Photoelectronics, Department of Physics, College of Science, Shantou University, Shantou 515063, China
3 Key Laboratory of Intelligent Manufacturing Technology of MOE, Shantou University, Shantou 515063, China
4 Key Laboratory of Specialty Fiber Optics and Optical Access Networks, Joint International Research Laboratory of Specialty Fiber Optics and Advanced Communication, Shanghai University, Shanghai 200444, China
5 DTU Electro, Department of Electrical and Photonics Engineering, Technical University of Denmark, 2800 Lyngby, Denmark
6 Center for Cognition and Neuroergonomics, State Key Laboratory of Cognitive Neuroscience and Learning, Beijing Normal University, Zhuhai 519087, China
7 Department of Electromagnetism and Telecommunication, University of Mons, Boulevard Dolez 31, 7000 Mons, Belgium
* Correspondence: wangheng@sau.edu.cn

Abstract: In this paper, the first- and fourth-order fiber Bragg grating (FBG)-based axial strain sensors are proposed. The FBGs are inscribed in step-index polymer optical fibers (POFs) (TOPAS core and ZEONEX cladding) via the point-by-point (PbP) direct-writing technique. A first-order FBG with a single peak is obtained with a pulse fluence of 7.16 J/cm^2, showing a strain sensitivity of 1.17 pm/με. After that, a fourth-order FBG with seven peaks is obtained with a pulse fluence of 1.81 J/cm^2 with a strain sensitivity between 1.249 pm/με and 1.296 pm/με. With a higher fluence of 2.41 J/cm^2, a second fourth-order FBG with five peaks is obtained, each of which is split into two peaks due to high birefringence (Hi-Bi) of ~5.4×10^{-4}. The two split peaks present a strain sensitivity of ~1.44 pm/με and ~1.55 pm/με, respectively. The peak difference corresponding to Hi-Bi presents a strain sensitivity of ~0.11 pm/με and could potentially be used for simultaneous dual-parameter measurement, such as temperature and strain.

Keywords: polymer optical fiber; fiber Bragg grating; birefringence; strain sensing

Citation: Gao, S.; Wang, H.; Chen, Y.; Wei, H.; Woyessa, G.; Bang, O.; Min, R.; Qu, H.; Caucheteur, C.; Hu, X. Point-by-Point Induced High Birefringence Polymer Optical Fiber Bragg Grating for Strain Measurement. *Photonics* **2023**, *10*, 91. https://doi.org/10.3390/photonics10010091

Received: 2 December 2022
Revised: 10 January 2023
Accepted: 12 January 2023
Published: 13 January 2023

1. Introduction

Since the first fabrication of fiber Bragg gratings (FBGs) in polymer optical fiber (POF) [1], FBGs have been successfully inscribed in various polymers, such as poly(methyl methacrylate) (PMMA) [1], the cyclic olefin copolymer (TOPAS Advanced Polymers, TOPAS) [2], the cyclic transparent amorphous fluoropolymer (Ashasi Glass, CYTOP) [3,4], the cyclic olefin polymer (ZEON CORPORATION, ZEONEX) [5], and polycarbonate (PC) [6]. Meanwhile, based on unique properties of POFs, i.e., a larger thermo-optic coefficient, a smaller Young's modulus, and good biocompatibility, POF-based FBG sensors have been widely used for different sensing applications, such as temperature, strain, humidity, and vital signs [5,7,8].

Compared to the phase-mask technology, which is most popular for mass production of FBGs, femtosecond direct-writing technology provides some unique advantages, including high accuracy and high quality with reduced thermal effect [9]. In 2012, Stefani et al. reported point-by-point (PbP) inscription of a fourth-order FBG in a microstructured POF (mPOF), which was asymmetrically designed such that the microstructure did not interfere

with the writing beam during inscription [10]. In 2015, Lacraz et al. inscribed a four-order FBG with a reflectivity of 70% in a CYTOP fiber via the line-by-line (LbL) technique [11]. In 2021, Dash et al. inscribed four-order FBGs in step-index rectangular ZEONEX POFs using a 520 nm femtosecond laser and the PbP technique [12]. The following year, Hu et al. produced first-order FBG in both BDK-doped POFs [13] and TOPAS/ZEONEX POFs [14].

In terms of strain measurements, PMMA is the most popular material, with a typical Young's modulus of 3.3 GPa with a failure strain over 100% and a yield strain of ~6% [7]. For FBG resonances at 850 nm and 1550 nm fabricated using a helium–cadmium (He-Cd) laser and the phase-mask technique in mPOFs and step-index POFs, the strain sensitivity was measured to be 0.71 pm/με at 850 nm and 1.3 pm/με at 1550 nm, respectively [15]. For FBG resonances at ~1530 nm inscribed using the same laser and technique in step-index POFs, the strain sensitivity was 1.34 pm/με and 1.2 pm/με, respectively, for 253 μm- and 16 μm-diameter fibers [16].

Additionally, TOPAS and ZEONEX are humidity-insensitive materials. For FBGs resonant at ~870 nm inscribed in TOPAS mPOFs using a He-Cd laser and the phase-mask technique, a strain sensitivity of 0.64 pm/με was obtained [17]. For the high-order FBGs inscribed in the ZEONEX POFs, the strain sensitivity was 0.731 pm/με and 1.29 nm/με at ~867 nm and ~1511 nm, respectively [12]. For the FBG at 870 nm inscribed in a step-index POF (TOPAS core and ZEONEX cladding) using a He-Cd laser and the phase-mask technique, a strain sensitivity of 0.76 pm/με with a maximal strain up to 3% was obtained [18].

Though POF-based FBG sensors present unique advantages for strain sensing, such as a large sensitivity [19] and sensing range, in practical applications temperature variations could interfere with the performance of these sensors. To measure the strain and temperature simultaneously, Oliveira fabricated a multimode interferometer with an FBG in the multimode POF and two single-mode silica fibers on both sides of the POF [20]. For the same purpose, Pereira et al. partially reduced the cross-sectional area by micromachining a slot using a femtosecond laser on the surface of the mPOF including an FBG [21].

In this paper, we use the femtosecond PbP technique to fabricate FBG axial strain sensors in single-mode step-index TOPAS/ZEONEX POFs. In the first regime with an objective lens (NA = 1.42), a first-order FBG with a single peak (FBG 1) is obtained with a pulse fluence of 7.16 J/cm^2, showing a sensitivity of 1.17 pm/με. In the second regime with an objective lens (NA = 0.75), a fourth-order FBG with seven grating peaks (FBG 2) is obtained with a pulse fluence of 1.81 J/cm^2, presenting a sensitivity between 1.249 pm/με and 1.296 pm/με. With a higher fluence of 2.41 J/cm^2, a second fourth-order FBG with five peaks (FBG 3) is obtained, each of which is split into two peaks due to high birefringence (Hi-Bi) of ~5.4×10^{-4}. The two split peaks show a strain sensitivity of ~1.44 pm/με and ~1.55 pm/με, respectively, and the split-peak distance corresponding to Hi-Bi shows a sensitivity of ~0.11 pm/με.

2. Axial Strain-Sensing Principles

An FBG works as a mirror reflecting light around the Bragg wavelength λ_{Bragg}, which depends on the effective refractive index of the core mode n_{eff} and the refractive-index modulation period Λ. The λ_{Bragg} is expressed as:

$$m\lambda_{Bragg} = 2n_{eff}\Lambda \quad (1)$$

where m represents the grating order. By applying an axial strain ε on an optical fiber, Λ is generally subject to the same strain, and n_{eff} is modified by the strain–optic effect [22]. Thus, according to Equation (1), the wavelength change $\Delta\lambda_{Bragg}$ due to strain variation $\Delta\varepsilon$ is given by

$$\Delta\lambda_{Bragg} = \lambda_{Bragg}(1 - p_e)\Delta\varepsilon \quad (2)$$

where p_e is the so-called effective strain–optic constant and is defined as:

$$p_e = -\frac{1}{n_{eff}}\frac{dn_{eff}}{d\varepsilon} = \frac{n_{eff}^2}{2}[p_{12} - v(p_{11} + p_{12})], \tag{3}$$

where p_{11} and p_{12} represent elements of the elasto-optic tensor, and v is the Poisson's ratio.

Due to the Hi-Bi, a single Bragg peak of an FBG in the reflected spectrum is split into two peaks, which correspond to two different n_{eff} at two orthogonal fiber axes, i.e., the slow and fast axis (s- and f-axis). Thus, according to Equation (1), the birefringence can be expressed as

$$n_{eff,s} - n_{eff,f} = \frac{m\left(\lambda_{Bragg,s} - \lambda_{Bragg,f}\right)}{2\Lambda} = \frac{m\lambda_D}{2\Lambda} \tag{4}$$

where $\lambda_{Bragg,s}$ and $\lambda_{Bragg,f}$ represent the wavelengths of two split peaks, and λ_D represents the peak difference. The wavelength shift of the Hi-Bi FBG as a function of axial strain is expressed as [23]

$$\Delta\lambda_{Bragg,s} = \lambda_{Bragg,s}\left\{1 + \frac{n_{eff,s}^2}{2}[v(p_{11} + p_{12}) - p_{12}]\right\}\Delta\varepsilon, \tag{5}$$

$$\Delta\lambda_{Bragg,f} = \lambda_{Bragg,f}\left\{1 + \frac{n_{eff,f}^2}{2}[v(p_{11} + p_{12}) - p_{12}]\right\}\Delta\varepsilon, \tag{6}$$

Consequently, the variation of the peak distance $\Delta\lambda_D$ can be obtained by Equations (5) and (6)

$$\Delta\lambda_D = \Delta\lambda_{Bragg,s} - \Delta\lambda_{Bragg,f} \tag{7}$$

3. FBG Inscription

3.1. Experimental Setup

FBGs were photo-inscribed in single-mode step-index TOPAS/ZEONEX POFs by the femtosecond laser PbP direct-writing technique. The fiber was developed in-house at DTU Electro, with core material TOPAS (5013S-04, TOPAS Advanced Polymers) and cladding material ZEONEX (480R, ZEON CORPORATION). The core and cladding diameter were 5 µm and 128 µm, respectively [18]. Compared to the case of writing FBG in mPOFs [10], the PbP inscription in step-index POFs in this work was easier to implement, as the fiber was symmetrically designed and fabricated. The laser micromachining system was from Newport Corporation, and contained a femtosecond laser (SpOne-8-SHG, Newport) emitting at 520 nm with a pulse duration of 306 fs and a maximal repetition rate of 200 kHz. The laser power could be altered by rotating a half-wave plate followed by a Glan laser polarizer. A quarter-wave plate was used to generate circularly polarized pulses to significantly reduce the anisotropy of the refractive index change. The laser beam was reflected by a dichroic mirror and then focused on the fiber by using an objective lens, which featured a magnification of 60× and an NA of 1.42 (UPLXAPO60XO, OLYMPUS) for the first regime and a magnification of 40× and an NA of 0.75 for the second regime. The diameter of the focused beam spot was estimated by the diffraction limit $D = 1.22\lambda/NA$ [24]. More information about the inscription setup can be found in our previous work [13]. LED illumination and a CCD camera were employed to capture the microscopic images of the refractive modification in real time. It is worth mentioning that actual size of the refractive-index modification is normally smaller than the beam diameter due to the refractive-index-modification threshold. For example, the estimated diameter of the refractive-index modification in FBG 1 was around 0.3 µm, whereas the beam spot had a diameter of 0.45 µm [14].

Before grating inscription, a ~3.5 cm-long piece of POF was connectorized to two silica-fiber pigtails with UV-curing glue. The POFs positioned under the objective lens

were fixed with two fiber holders, which were mounted on three-axis precision-translation stages (X/Y: XMS100-S, Z: M-VP-5ZA, Newport). The FBG inscription setup is illustrated in Figure 1. The grating period Λ is equal to the ratio of the translation velocity v to the pulse repetition rate f. In this work, the translation velocity was adjustable, and the pulse-repetition rate was set to a constant value of 50 Hz. The reflected grating spectra of FBGs 1–2 were monitored by an FBG interrogator system (FS22SI, HBM FiberSensing) featuring a wavelength resolution of 1 pm and a scanning rate of 1 Hz. The counterparts of FBG 3 were interrogated using a broadband source (ASE-C+L LIGHT SOURCE, Golight) and an optical-spectrum analyzer (Anritsu MS9740A). The data of the grating inscriptions are displayed in Table 1.

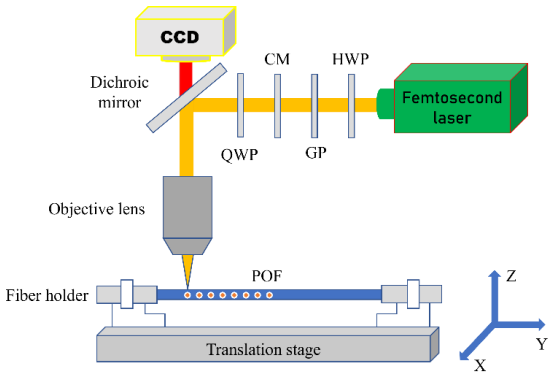

Figure 1. Schematic of the experimental setup for PbP FBG inscription in POP. HWP: half-waveplate, GP: Glan polarizer, CM: collimator, QWP: quarter-waveplate.

Table 1. Data of grating inscriptions by the femtosecond laser at 520 nm.

Regime	**1**	**2**	
NA of objective lens	1.42	0.75	
FBG	1	2	3
Pulse energy (nJ)	11.22	10.15	13.54
Focused-beam diameter (μm)	0.45	0.85	0.85
Pulse fluence (J/cm^2)	7.16	1.81	2.41
Translation velocity (μm/s)	25.95	101	100
Grating length (mm)	2	4	4
Grating period (μm)	0.519	2.02	2
Bragg wavelength (nm)	1584	1522~1582	1520~1540

3.2. Experimental Results

In the first regime, a 2 mm-long FBG 1 was inscribed with a pulse energy of 11.22 nJ. The reflected spectrum is shown in Figure 2, showing a single grating peak at 1584 nm. Good stability of the FBGs inscribed in the same type of fiber using the same technique was already demonstrated and reported in our previous work [14]. In the second regime, the 4 mm-long FBG 2 was obtained with a pulse energy of 10.15 nJ, and seven grating peaks were presented with a peak distance of ~9.8 nm, as shown in Figure 3. The comb-like spectrum with regularly spaced resonances could be attributed to the generation of sampled FBGs, resulting from the minor core-cladding eccentricity due to the fiber imperfection during the fiber-fabrication process and the unwanted helically twisted structure in the fiber-mounting process. A similar FBG spectrum was demonstrated in helically twisted silica optical fiber [25]. It is worth mentioning that the generation of multipeak behavior is also sensitive to the grating orders, as first-order FBG (FBG 1) showed only one peak. A similar situation was found in largely chirped-structure FBGs [26]. Further investigation will be conducted in future work. The mechanism for multi-peak generation in this work is different from that using a phase mask with higher diffraction orders [27]. Besides, for

an elevated pulse energy of 13.54 nJ, the 4 mm-long FBG 3 was achieved with five main grating peaks with a peak distance of ~5.8 nm. Each of them was split into two main peaks, as shown in Figure 4. This phenomenon, which was not observed for FBG 2 and with lower pulse fluence, could be due to Hi-Bi induced by higher pulse fluence.

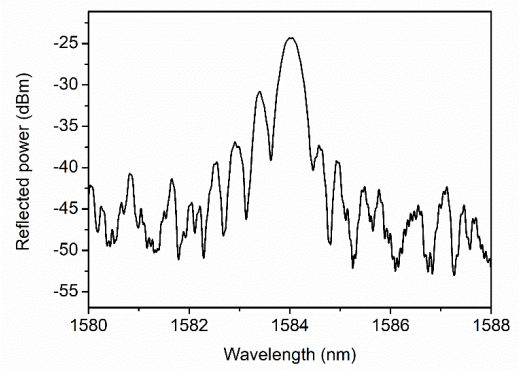

Figure 2. Reflected spectrum of the 2 mm-long FBG inscribed with a pulse energy of 11.22 nJ in the first regime.

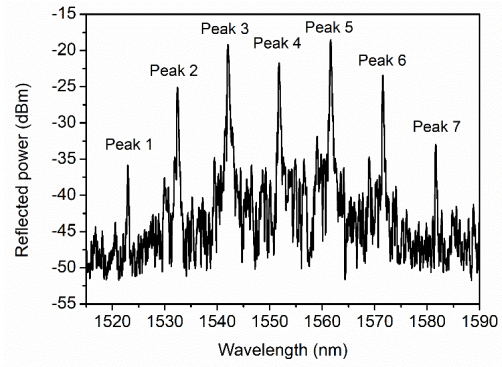

Figure 3. Reflected spectrum of the 4 mm-long FBG inscribed with a pulse energy of 10.15 nJ in the second regime.

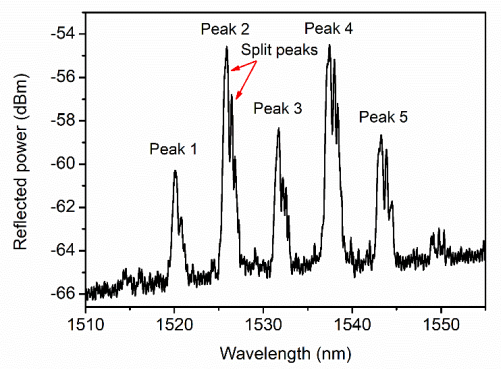

Figure 4. Reflected spectrum of the 4 mm-long FBG inscribed with a pulse energy of 13.54 nJ in the second regime.

The distances of the split peaks of FBG 3 were 0.63 nm, 0.55 nm, 0.48 nm, 0.54 nm, and 0.57 nm for peaks 1–5, respectively, yielding a birefringence value approximately equal to 6.3×10^{-4}, 5.5×10^{-4}, 4.8×10^{-4}, 5.4×10^{-4}, and 5.7×10^{-4}, respectively, according to Equation (4). This birefringence is one order of magnitude higher than that reported in our previous work, where a birefringence of 3.0×10^{-5} was induced in PMMA mPOF during the FBG inscription with the phase-mask technique [28], because the focused beam spot on the fiber core for the femtosecond PbP method in this work was much smaller than the

counterpart in the phase-mask technique, inducing more inhomogeneous refractive-index modifications. In addition, the birefringence obtained in this work was somewhat less than the 7.93×10^{-4} obtained in the standard single-mode silica optical fiber via the line-by-line FBG inscription technique [29].

4. Axial Strain Measurements

4.1. Experimental Setup

During the axial strain measurement, both the room temperature and relative humidity were under control, which were kept constant at 25 °C and 40%, respectively. The experimental setup is shown in Figure 5. A three-axis translation stage (MBT616D/M, Thorlabs) with a fine travel range of 300 μm was used for this axial strain measurement. Both sides of the POF adjacent to the splice point of the POF and the silica fiber were permanently fixed on the fiber clamps using UV-glue so the strain was accurately applied to the POF.

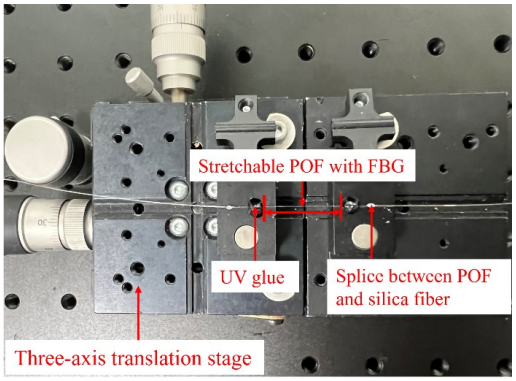

Figure 5. Experimental setup for strain measurement.

4.2. Experimental Results

For FBG 1 obtained in the first regime, the strain introduced to the fiber was increased from 0% to 1.08%. The spectrum response to the applied strain is depicted in Figure 6a, and the Bragg wavelength versus strain is displayed in Figure 6b, showing a linear strain response with a sensitivity of 1.17 pm/με ± 0.02 pm/με via linear regression. For FBG 2 obtained in the second regime, the strain applied to the fiber was set from 0% to 1.05%. The spectra of peaks 1–7 in terms of strain are shown in Figure 7a–g, respectively, and the shifts in the Bragg wavelengths in response to the strains are shown in Figure 7h. After linear regression, the sensitivity (slope) is shown in Table 2. It was found that the strain sensitivity increased with the Bragg wavelength, from 1.249 pm/με for ~peak 1 to 1.296 pm/με for peak 7.

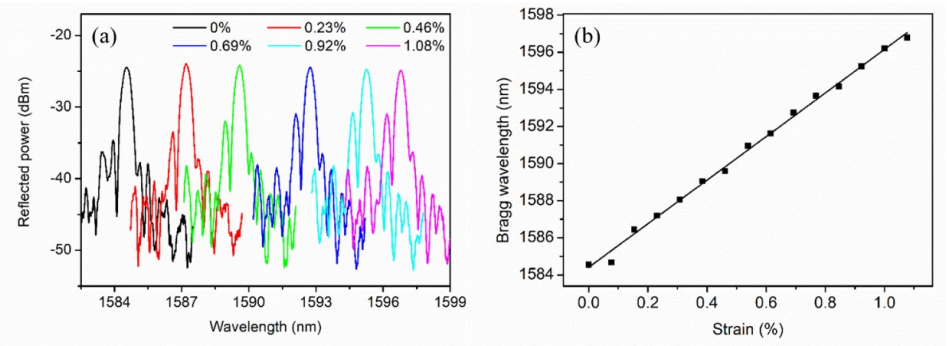

Figure 6. The spectrum (**a**) and Bragg wavelength shift (**b**) in terms of the strain from 0% to 1.08% for FBG 1 in the first regime.

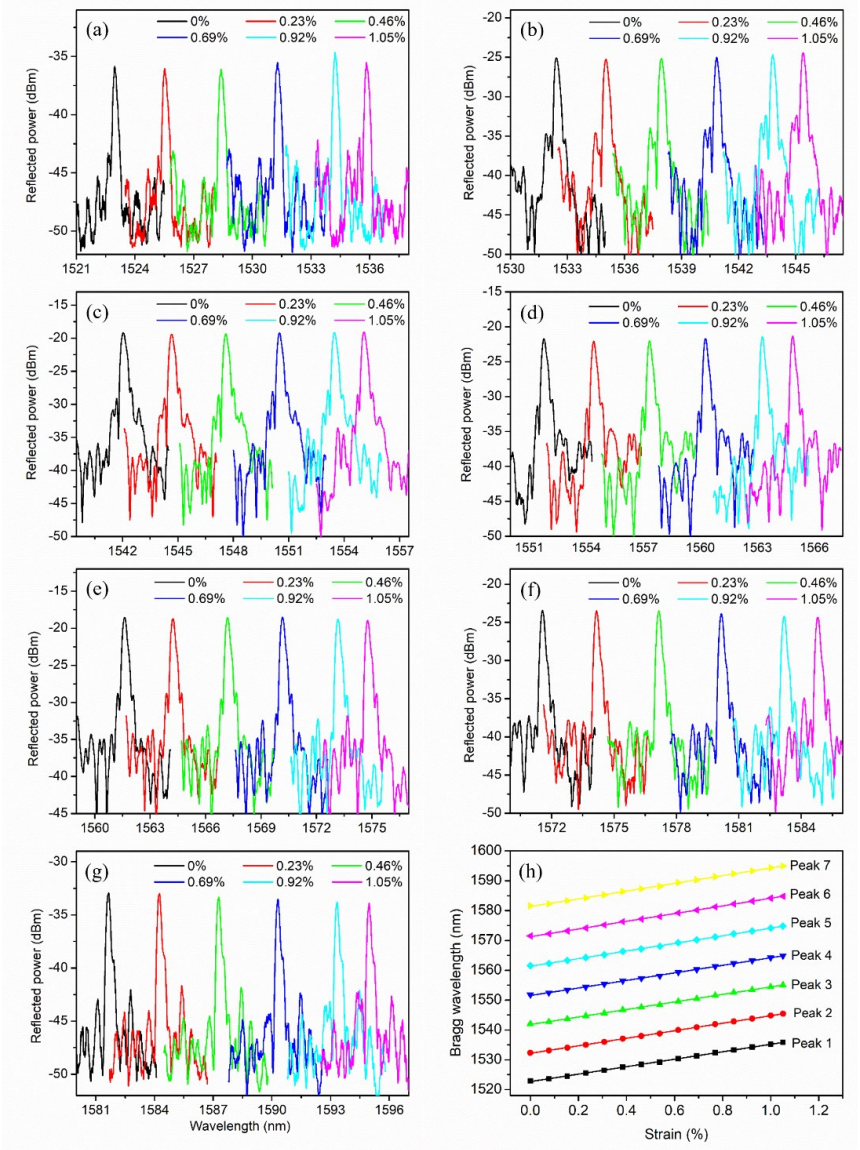

Figure 7. The spectra of peaks 1–7 (**a**–**g**) and Bragg wavelength shift (**h**) in terms of the strain from 0% to 1.05% for FBG 2 in the second regime.

Table 2. Linear fit of peaks 1–7 of FBG 2 in the first regime as a function of strain from 0% to 1.05%.

Peak	1	2	3	4	5	6	7
Slope (pm/με)	1.249	1.260	1.262	1.267	1.276	1.287	1.296
Standard error (pm/με)	0.008	0.007	0.008	0.008	0.008	0.008	0.008

For FBG 3 obtained in the second regime, the strain introduced to the fiber was increased from 0% to 1.037%. The spectra of peaks 1–5 in terms of strain are shown in Figure 8a–e, respectively, and the Bragg wavelength shifts of the split peaks for peaks 1–5 are shown in Figure 8f–j, respectively. Different from FBGs 1 and 2, the evolution of the Bragg wavelength of the split peaks in terms of strain was nonlinear (second-order polynomial fit). It was found that the strain sensitivity decreased when the strain increased. The nonlinear strain sensitivity could be attributed to the strain-dependent parameters p_{11}, p_{12}, and v. Based on the fit curves of the two split peaks, the difference was calculated, presenting increasing properties as a function of strain, as shown in Figure 8f–j for peaks 1–5, respectively. For the strain of 1.037%, the largest λ_D of FBG 3 were obtained, which were

1.40 nm, 1.53 nm, 1.17 nm, 1.51 nm, and 1.66 nm for peaks 1–5, respectively. The spectrum with two split peaks was similar to the one demonstrated in Ref. [29]. The variation of λ_D could be attributed to the change in Hi-Bi induced by the increasing strain, similar to the cases reported in Refs. [30,31]. According to Equations (5) and (6), the wavelength shifts as a function of strain could have been inconsistent, as the parameters p_{11}, p_{12}, and v could have been influenced differently by the asymmetric laser modifications. Consequently, the birefringence value for each peak was approximately equal to 1.40×10^{-3}, 1.53×10^{-3}, 1.17×10^{-3}, 1.51×10^{-3}, and 1.66×10^{-3}, respectively, according to Equation (4).

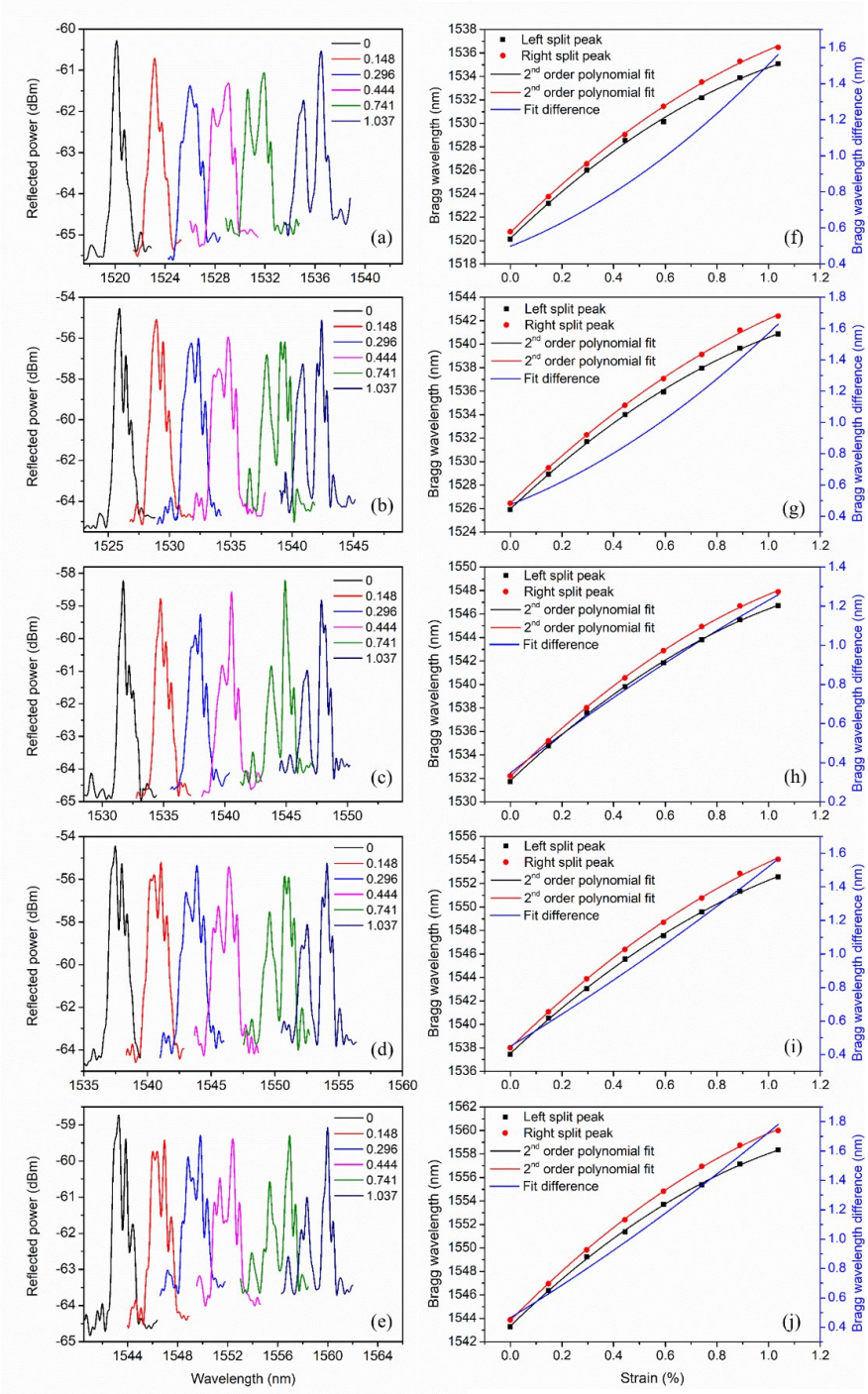

Figure 8. The spectra of peaks 1–5 (**a**–**e**) and the Bragg wavelength shift of the split peaks for peaks 1–5 (**f**–**j**) in terms of the strain from 0% to 1.037% for FBG 3 in the second regime.

It is worth mentioning that for FBG 1 and 2, the smaller side peaks in the reflected spectra adjacent to the highest peaks were considered the side lobes of the gratings, which move with the highest peaks, showing similar sensitivities in terms of strain. However, for FBG 3, the distance between the two split peaks increased as a function of strain. The peak distortion could be attributed to the interference from the grating side lobes. Thus, we believe that unlike the cases for FBG 1 and 2, emergence of the split peaks in the reflection spectra of FBG3 was due to the high birefringence in the FBG. In addition, these multi-peaks should not be associated with the few-mode behavior of the fiber associated with the higher fluency because of two reasons: (1) negative effective refractive-index modification was obtained in the same fiber [14], and (2) FBG resonances in few-mode fiber showed quite similar strain sensitivities [32].

Though the split peaks in terms of strain presented nonlinear properties, to better characterize the performance of this strain sensor, the linear sensitivity was further calculated by linear fit based on the raw data of the split peaks, showing a similar strain sensitivity of ~1.44 pm/με and ~1.55 pm/με, respectively, and their Bragg wavelength difference λ_D versus strain varied, with a similar sensitivity of ~0.11 pm/με, which is five times as high as the 0.0214 pm/με obtained using the sawtooth stressor-assisted Hi-Bi FBG [30]. The slopes and the standard errors for peaks 1–5 after linear fit are presented in Table 3. Since the split peaks and λ_D presented very different strain sensitivities, the Hi-Bi FBG sensor could be potentially used to measure strain and temperature simultaneously [30,31].

Table 3. Linear fit of peaks 1–5 of FBG 3, including left and right split peaks and their difference in the second regime as a function of strain from 0% to 1.037%.

Peak		1	2	3	4	5
Left split peak	Slope (pm/με)	1.43	1.44	1.44	1.46	1.45
	Standard error (pm/με)	0.08	0.07	0.08	0.07	0.08
Right split peak	Slope (pm/με)	1.54	1.55	1.53	1.56	1.57
	Standard error (pm/με)	0.08	0.07	0.08	0.07	0.08
λ_D	Slope (pm/με)	0.10	0.11	0.09	0.11	0.13
	Standard error (pm/με)	0.02	0.01	0.01	0.01	0.02

5. Conclusions

In this work, 2 mm-long FBG-based axial strain sensors in step-index TOPAS/ZEONEX POFs are proposed. The FBGs were inscribed by the femtosecond PbP direct-writing technique at 520 nm in two regimes. In the first regime with an objective lens (NA = 1.42), a first-order FBG with a single peak (FBG 1) was obtained with a pulse fluence of 7.16 J/cm^2, showing a linear strain sensitivity of 1.17 pm/με in the range of 0 to 1.08%. In the second regime with an objective lens (NA = 0.75), a fourth-order FBG with seven peaks (FBG 2) was obtained with a pulse fluence of 1.81 J/cm^2, presenting a linear strain response with a sensitivity between 1.249 pm/με and 1.296 pm/με in the range of 0 to 1.05%. With a higher fluence of 2.41 J/cm^2, a second fourth-order FBG with five peaks (FBG 3) was obtained, each of which was split to two peaks due to Hi-Bi being equal to 6.3×10^{-4}, 5.5×10^{-4}, 4.8×10^{-4}, 5.4×10^{-4}, and 5.7×10^{-4}, respectively. The two split peaks of the five peaks presented nonlinear (second-order polynomial fit) strain response with a similar strain sensitivity of ~1.44 pm/με and ~1.55 pm/με, respectively, after linear fit, and their Bragg wavelength difference versus strain varied, with a similar sensitivity of ~0.11 pm/με in the range of 0 to 1.037%. At the strain of 1.037%, the largest birefringence values were 1.40×10^{-3}, 1.53×10^{-3}, 1.17×10^{-3}, 1.51×10^{-3}, and 1.66×10^{-3}, respectively. This Hi-Bi FBG sensor could be potentially used to measure strain and temperature simultaneously.

Author Contributions: Conceptualization, H.W. (Heng Wang) and X.H.; methodology, S.G. and Y.C.; validation, S.G., H.W. (Heng Wang) and Y.C.; investigation, H.W. (Heming Wei), G.W., R.M. and H.Q.; writing—original draft preparation, S.G., H.W. (Heng Wang) and X.H.; writing—review and editing, H.W. (Heming Wei), G.W., O.B., R.M., H.Q. and C.C.; supervision, H.W. (Heng Wang) and X.H.; funding acquisition, H.W. (Heng Wang), X.H., H.Q. and C.C. All authors have read and agreed to the published version of the manuscript.

Funding: This work is supported by scientific research project of Liaoning Provincial Education Department (No. LJKMZ 20220544), Special projects in key fields of colleges and universities in Guangdong Province (No. 2020ZDZX3037), Science and Technology Department of Guangdong Province (No. 2022A1515012571), and the Fonds de la Recherche Scientifique (F.R.S.-FNRS) under the Postdoctoral Researcher Grant (Chargé de Recherches) of Xuehao Hu and the Senior Research Associate Position of Christophe Caucheteur.

Institutional Review Board Statement: Not applicable.

Informed Consent Statement: Not applicable.

Data Availability Statement: Data underlying the results presented in this paper are not publicly available at this time but may be obtained from the authors upon reasonable request.

Conflicts of Interest: The authors declare no conflict of interest.

References

1. Xiong, Z.; Peng, G.D.; Wu, B.; Chu, P.L. Highly tunable Bragg gratings in single-mode polymer optical fibers. *IEEE Photon. Technol. Lett.* **1999**, *11*, 352–354. [CrossRef]
2. Johnson, I.P.; Yuan, W.; Stefani, A.; Nielsen, K.; Rasmussen, H.K.; Khan, L.; Webb, D.J.; Kalli, K.; Bang, O. Optical fibre Bragg grating recorded in TOPAS cyclic olefin copolymer. *Electron. Lett.* **2011**, *47*, 271. [CrossRef]
3. Nan, Y.-G.; Kinet, D.; Chan, K.; Chapalo, I.; Caucheteur, C.; Megret, P. Ultra-fast fiber Bragg grating inscription in CYTOP polymer optical fibers using phase mask and 400 nm femtosecond laser. *Opt. Express.* **2021**, *29*, 25824. [CrossRef]
4. Theodosiou, A.; Kalli, K. Recent trends and advances of fibre Bragg grating sensors in CYTOP polymer optical fibres. *Opt. Fiber Technol.* **2020**, *54*, 102079. [CrossRef]
5. Woyessa, G.; Fasano, A.; Markos, C.; Stefani, A.; Rasmussen, H.K.; Bang, O. Zeonex microstructured polymer optical fiber: Fabrication friendly fibers for high temperature and humidity insensitive Bragg grating sensing. *Opt. Mater. Express.* **2017**, *7*, 286. [CrossRef]
6. Fasano, A.; Woyessa, G.; Stajanca, P.; Markos, C.; Stefani, A.; Nielsen, K.; Rasmussen, H.K.; Krebber, K.; Bang, O. Fabrication and characterization of polycarbonate microstructured polymer optical fibers for high-temperature-resistant fiber Bragg grating strain sensors. *Opt. Mater. Express.* **2016**, *6*, 649–659. [CrossRef]
7. Webb, D.J. Fibre Bragg grating sensors in polymer optical fibres. *Meas. Sci. Technol.* **2015**, *26*, 092004. [CrossRef]
8. Theodosiou, A.; Lacraz, A.; Stassis, A.; Koutsides, C.; Komodromos, M.; Kalli, K. Plane-by-Plane femtosecond laser inscription method for single-peak Bragg gratings in multimode CYTOP polymer optical fiber. *J. Light. Technol.* **2017**, *35*, 5404–5410. [CrossRef]
9. Beresna, M.; GeceviIus, M.; Kazansky, P.G. Ultrafast laser direct writing and nanostructuring in transparent materials. *Adv. Opt. Photon.* **2014**, *6*, 293.
10. Stefani, A.; Stecher, M.; Town, G.E.; Bang, O. Direct Writing of Fiber Bragg Grating in Microstructured Polymer Optical Fiber. *IEEE Photon. Technol. Lett.* **2012**, *24*, 1148–1150. [CrossRef]
11. Lacraz, A.; Polis, M.; Theodosiou, A.; Koutsides, C.; Kalli, K. Femtosecond Laser Inscribed Bragg Gratings in Low Loss CYTOP Polymer Optical Fiber. *IEEE Photonics Technol. Lett.* **2015**, *27*, 693. [CrossRef]
12. Dash, J.N.; Cheng, X.; Gunawardena, D.S.; Tam, H.-Y. Rectangular single-mode polymer optical fiber for femtosecond laser inscription of FBGs. *Photonics Res.* **2021**, *9*, 1931–1938.
13. Hu, X.; Chen, Z.; Cheng, X.; Min, R.; Qu, H.; Caucheteur, C.; Tam, H.-Y. Femtosecond laser point-by-point Bragg grating inscription in BDK-doped step-index PMMA optical fibers. *Opt. Lett.* **2022**, *47*, 249. [CrossRef] [PubMed]
14. Hu, X.; Chen, Y.; Gao, S.; Min, R.; Woyessa, G.; Bang, O.; Qu, H.; Wang, H.; Caucheteur, C. Direct Bragg grating inscription in single mode step-index TOPAS/ZEONEX polymer optical fiber using 520 nm femtosecond pulses. *Polymers.* **2022**, *14*, 1350. [CrossRef] [PubMed]
15. Abang, A.; Webb, D.J. Influence of mounting on the hysteresis of polymer fiber Bragg grating strain sensors. *Opt. Lett.* **2013**, *38*, 1376–1378. [CrossRef]
16. Rajan, G.; Noor, M.Y.M.; Lovell, N.H.; Ambikaizrajah, E.; Farrell, G.; Peng, G.-D. Polymer micro-fiber Bragg grating. *Opt. Lett.* **2013**, *38*, 3359–3362. [CrossRef]
17. Yuan, W.; Khan, L.; Webb, D.J.; Kalli, K.; Rasmussen, H.K.; Stefani, A.; Bang, O. Humidity insensitive TOPAS polymer fiber Bragg grating sensor. *Opt. Express.* **2011**, *19*, 19731–19739. [CrossRef]

18. Woyessa, G.; Fasano, A.; Stefani, A.; Markos, C.; Nielsen, K.; Rasmussen, H.K.; Bang, O. Single mode step-index polymer optical fiber for humidity insensitive high temperature fiber Bragg grating sensors. *Opt. Express.* **2016**, *24*, 1253–1260. [CrossRef]
19. Stefani, A.; Andresen, S.; Yuan, W.; Herholdt-Rasmussen, N.; Bang, O. High Sensitivity Polymer Optical Fiber-Bragg-Grating-Based Accelerometer. *IEEE Photon. Technol. Lett.* **2012**, *24*, 763. [CrossRef]
20. Oliveira, R.; Marques, T.H.R.; Bilro, L.; Nogueira, R.; Cordeiro, C.M.B. Multiparameter POF sensing based on multimode interference and fiber Bragg grating. *J. Light. Technol.* **2016**, *35*, 3–9. [CrossRef]
21. Pereira, L.; Min, R.; Paixão, T.; Marques, C.; Woyessa, G.; Bang, O.; Pinto, J.L.; Antunes, P.F.d.C. Compact dual-strain sensitivity polymer optical fiber grating for multi-parameter sensing. *J. Light. Technol.* **2021**, *39*, 2230. [CrossRef]
22. Bertholds, A.; Dandliker, R. Determination of the individual strain optic coefficients in single-mode optical fibres. *J. Light. Technol.* **1988**, *6*, 17. [CrossRef]
23. Wang, Y.; Yun, B.; Chen, N.; Cui, Y. Characterization of a high birefringence fibre Bragg grating sensor subjected to nonhomogeneous transverse strain fields. *Meas. Sci. Technol.* **2006**, *17*, 939. [CrossRef]
24. Cao, Y.; Wood, S.; Richheimer, F.; Blakesley, J.; Young, R.J.; Castro, F.A. Enhancing and quantifying spatial homogeneity in monolayer WS2. *Sci. Rep.* **2021**, *11*, 14831. [CrossRef] [PubMed]
25. Li, J.; Chen, G.; Ma, P.; Sun, L.; Wu, C.; Guan, B. Sampled Bragg gratings formed in helically twisted fibers and their potential application for the simultaneous measurement of mechanical torsion and temperature. *Opt. Express.* **2018**, *26*, 12903–12911. [CrossRef]
26. Chen, C.; Zhang, X.-Y.; Wei, W.-H.; Chen, Y.-Y.; Qin, L.; Ning, Y.-Q.; Yu, Y.-S. Multi-resonance peaks fiber Bragg gratings based on largely-chirped structure. *Opt. Commun.* **2018**, *412*, 150–154. [CrossRef]
27. Statkiewicz-Barabach, G.; Tarnowski, K.; Kowal, D.; Mergo, P.; Urbanczyk, W. Fabrication of multiple Bragg gratings in microstructured polymer fibers using a phase mask with several diffraction orders. *Opt. Express.* **2013**, *21*, 8521–8534. [CrossRef]
28. Hu, X.; Saez-Rodriguez, D.; Marques, C.; Bang, O.; Webb, D.J.; Mégret, P.; Caucheteur, C. Polarization effects in polymer FBGs: Study and use for transverse force sensing. *Opt. Express.* **2015**, *23*, 4581. [CrossRef]
29. Chah, K.; Kinet, D.; Wuilpart, M.; Mégret, P.; Caucheteur, C. Femtosecond-laser-induced highly birefringent Bragg gratings in standard optical fiber. *Opt. Letters.* **2013**, *38*, 594–596. [CrossRef]
30. Guo, K.; He, J.; Shao, L.; Xu, G.; Wang, Y. Simultaneous measurement of strain and temperature by a sawtooth stressor-assisted highly birefringent fiber Bragg grating. *J. Light. Technol.* **2019**, *38*, 2060–2066. [CrossRef]
31. Oh, S.T.; Han, W.T.; Paek, U.C.; Chung, Y. Discrimination of temperature and strain with a single FBG based on the birefringence effect. *Opt. Express* **2004**, *12*, 724–729. [CrossRef] [PubMed]
32. Huang, T.; Fu, S.; Ke, C.; Shum, P.P.; Liu, D. Characterization of fiber Bragg grating inscribed in few-mode silica-germanate fiber. *IEEE Photon. Technol. Lett.* **2014**, *26*, 1908–1911. [CrossRef]